Journal of Sound and Vibration (1999) **219**(2), 239–253
Article No. jsvi.1998.1883, available online at http://www.idealibrary.com.on IDEAL

ON THE MODELLING OF NON-LINEAR ELASTOMERIC VIBRATION ISOLATORS

A. K. Mallik, V. Kher, M. Puri† and H. Hatwal

Department of Mechanical Engineering, *Indian Institute of Technology*, *Kanpur*-208016, *India*

(*Received* 1 *September* 1997, *and in final form* 10 *July* 1998)

Vibration isolators consisting of polymeric materials exhibit non-linearity in their stiffness and damping characteristics. Two different approaches towards modelling these non-linear characteristics are discussed. In one approach, experimentally obtained hysteresis loops are modelled through a suitable constitutive equation. In the other, experimentally obtained harmonic, displacement transmissibility plots are modelled by expressing the restoring and damping forces through lower order polynomials of deformation and rate of deformation, respectively. In both cases, it is observed that the dynamic stiffness, which is more than the static stiffness, exhibits a small softening type non-linearity. The non-linearity in the damping characteristic is seen to be more pronounced than that in the stiffness.

1. INTRODUCTION

The highly deformable materials of long-chain molecules, referred to as elastomeric polymers, are extensively used in various forms for vibration control. One common application is in the form of a vibration isolator. Viscoelastic materials can be used to construct the so-called rubber-spring in various configurations, e.g., mat, waster and tube [1]. Further, elastomers are chemically bonded to metal parts giving rise to ready-to-use isolators. These bonded rubber springs are often used in the installation of machinery and equipment [2].

The distinguishing features of an elastomer, which make it useful for controlling the vibration, are its enormous resilience and high energy dissipation capacity. Moreover, the recent advances in polymer technology, like interpenetrating polymer networks (IPN), can impart almost tailor-made mechanical properties to a polymer [3]. Besides frequency and temperature dependence, the stiffness and damping characteristics also show non-linear characteristics [4, 5]. Mathematical models for these non-linear characteristics are required for estimating the performance of an elastomeric isolator.

In this paper two different approaches to obtaining these models are discussed, each serving a particular purpose. In the first one, an isolator is subjected to a

† On leave from Indian Navy.

0022–460X/99/020239 + 15 $30.00/0

harmonic loading, and the mechanical hysteresis loop is obtained by plotting the instantaneous force versus deformation over a cycle. This method was used by Tinker and Cutchins [6] for modelling a wire-rope vibration isolator. A mathematical expression correlating the force with the deformation and rate of deformation is attempted so as to simulate the experimentally obtained hysteresis loops. It is well known that different additives in the elastomer affect the shape and size of the hysteresis loop [7, 8]. Thus the experimentally obtained hysteresis loops may suggest to the rubber technologist how to improve the dynamic characteristics of the isolator. On the other hand, however, the mathematical model so resulting often turns out to be too complicated for further performance analysis of such non-linear isolators.

In the second approach, a single-degree-of-freedom system is fabricated by inserting the isolator between a rigid mass and a harmonically moving base. Then the harmonic, displacement transmissibility is measured at various exciting frequencies. The restoring and damping forces exerted by the isolator are assumed to be low order polynomial function, of its deformation and rate of deformation respectively. The exponents of the polynomials are chosen after a few trials. The coefficients of the polynomials are obtained by fitting the theoretical transmissibility plots with the experimentally obtained ones. Various analytical/numerical methods of obtaining the (theoretical) transmissibility with various types of non-linear isolators have already been reported [9, 10]. This approach thus results in a mathematical model which is convenient for further use in any non-linear analysis. However, no insight is gained about the mechanisms of energy dissipation which can help to modify the elastomer so as to improve its performance. Furthermore, the accuracy and range of validity of the model depend on the chosen values of the exponents.

In this paper, the first approach is discussed with reference to a tubular rubber (sleeve) specimen. The second approach is detailed with reference to a commercial bonded rubber spring in which the elastomer is bonded between a pair of leaf springs. The experimental details and results not included in this paper can be found in references [11, 12].

2. EXPERIMENTAL SET-UP AND METHOD

2.1. TUBULAR RUBBER SPECIMEN

The objective is to obtain the dynamic constitutive equation, for a tubular rubber specimen, which fits the hysteresis loops generated experimentally with various amplitudes and frequencies of harmonic loading. The specimen was made of natural rubber with carbon black fillers (IRHD 40). The external and internal diameters of the specimen were 34·8 mm and 21·2 mm respectively. The length of the specimen was 98·1 mm. A single-degree-of-freedom vibratory system was fabricated with this specimen as detailed below.

The specimen was attached at one end to a small cylindrical projection in a cast iron plate through a hose clamp. This assembly was fixed to a housing. Slots in the housing were used to guide projections in the cast iron plate. This, in turn,

reduced the movements of the specimen in transverse directions. The base of the housing also had a cylindrical projection at its centre to which the other end of the specimen was attached through another hose clamp. The housing was secured to a base plate which, in turn, was mounted on an electrodynamic shaker. A mild steel block was rigidly connected atop the cast iron plate.

When the shaker moves, the inertia force of the total mass (m) of the cast iron plate and the mild steel block is the external (harmonic) dynamic force acting on the rubber specimen. This inertia force is obtained by measuring the acceleration of the top block. The deformation of the specimen is obtained through simultaneous measurements of displacements of the top mass (x) and the base plate (y). The difference of these two displacements, obtained by using the subtraction mode of the oscilloscope, gives the instantaneous deformation $z(=x-y)$. The self-explanatory block diagram of the instrumentation used is shown in Figure 1. It may be mentioned that, in general, subtraction of two accelerometer signals is not recommended due to variations in their phase difference and transverse sensitivity. However, in the set-up used, the transverse movements were negligible. Moreover, experiments were conducted only up to 200 Hz, where as the usable range of the two identical accelerometers (measuring signals of the same frequency) is up to 6 kHz. Consequently, both the phase difference and the transverse sensitivity were negligible. The signals to the oscilloscope were digitized to 4096 data points and transferred to a PC through RS 232C. The oscilloscope had only 2 channels but three signals, viz., the base displacement, the displacement and acceleration of the top mass, were to be handled. Consequently, the phase compatibility between the acceleration and displacement of the top mass (180° out of phase) had to be maintained by proper synchronization during the processing of these three signals [11]. The natural frequency of the system was found to be around 57 Hz and experiments were conducted up to a maximum frequency of 200 Hz. The high frequency noise in all the signals was cut off by using a low-pass fitter. The cut off frequency of the low-pass fitter was set at 3 kHz. The static stiffness of the (encased) specimen was obtained by conducting a compression test in a Universal Testing Machine INSTRON 1195.

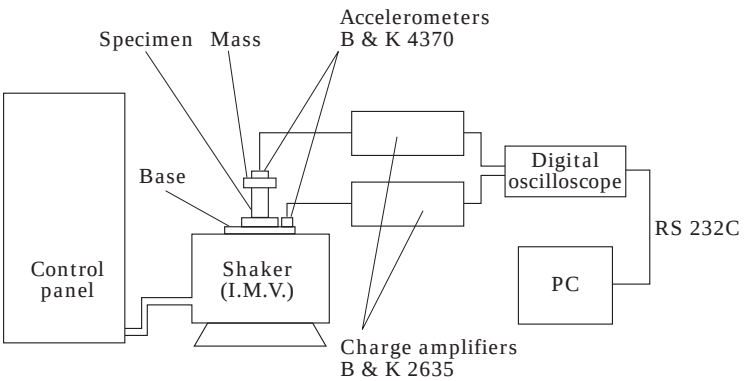

Figure 1. Block diagram of instrumentation.

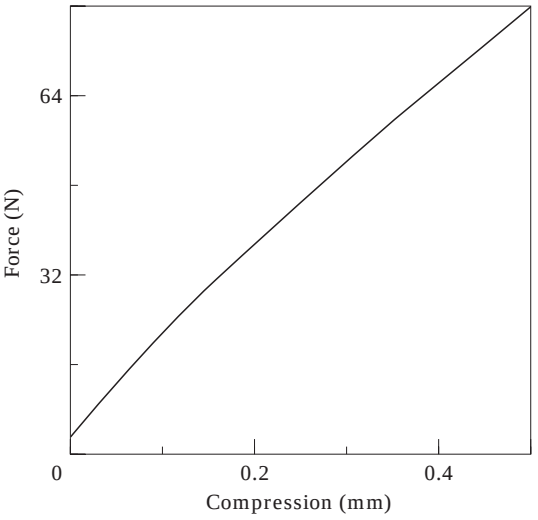

Figure 2. Static force–deformation characteristic during compression test of the tubular specimen.

2.2. BONDED RUBBER SPRING

The specimen used was a commercial metal bonded rubber spring (No. X-20, manufactured by Resistoflex, India) where the elastomer is bonded between a pair of leaf springs. Again a single-degree-of-freedom system with harmonic base excitation was fabricated. A rigid block was attached to the top of the spring whereas the bottom of the spring was connected to the shaker table through a base plate. The amplitudes of the top mass (X) and the base plate (Y) were simultaneously measured by using accelerometers and charge amplifiers as explained in section 2.1. The displacement transmissibility $T = (X/Y)$ was measured at various excitation frequencies covering the resonance zone. Similar measurements were carried out with different base amplitudes. It is well known that for non-linear systems, the harmonic, displacement transmissibility depends on the base amplitude [13]. The static stiffness of the specimen was also obtained by conducting a compression test in INSTRON 1195.

3. RESULTS AND DISCUSSIONS

3.1. TUBULAR RUBBER SPECIMEN

Figure 2 shows the force–deformation curve during the static test. A slight softening type characteristic is evident from this figure. Figure 3 shows the hysteresis loops at three different frequencies with identical deformation amplitude. The base amplitudes were adjusted so as to generate the same amplitude of deformation. The slope of the backbone curve of the hysterics loop indicates the dynamic stiffness of the specimen. This backbone curve is obtained by joining the points which indicate the average values of the external forces during loading and unloading for a given deformation. The area of the mechanical hysteresis loop signifies the specific damping energy (D_s) of the specimen which

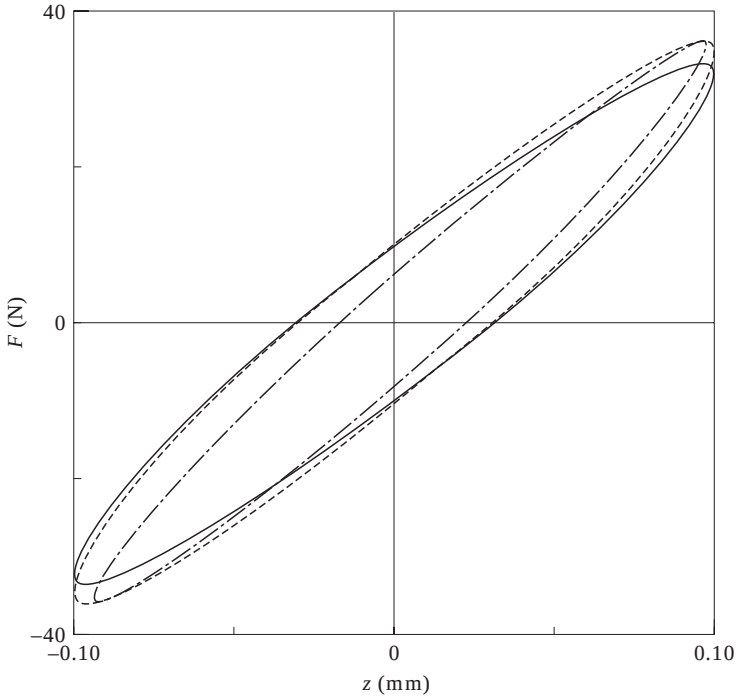

Figure 3. Mechanical hysteresis loops with 0·1 mm deformation amplitude at different frequencies: ——, 50 Hz; ----, 90 Hz; – · –, 150 Hz.

is the energy dissipated by the specimen per cycle. The area of the hysteresis loop was calculated using the trapezoidal rule on the data points stored in the PC.

Figure 4 shows the variation of D_s with the excitation frequency (ω) for a constant deformation amplitude. It may be concluded from Figures 3 and 4 that neither the dynamic stiffness nor the damping force changes substantially with frequency (within the range of measurement, i.e., 20–200 Hz). Thus the hysteretic and Coulomb, rather than the viscous (frequency dependent), damping mechanisms seem to be predominant.

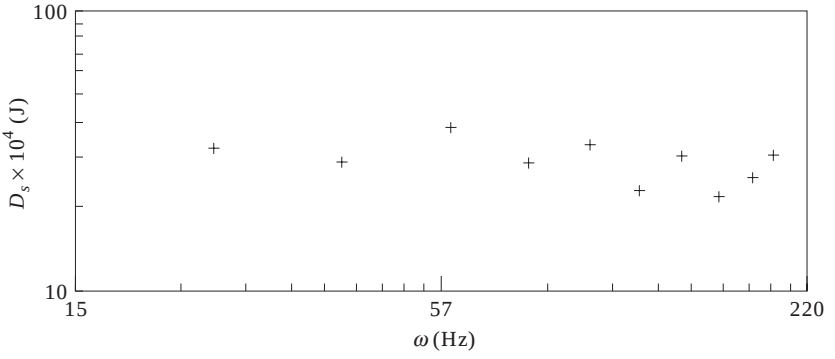

Figure 4. Variation of the specific damping energy with the excitation frequency at a deformation–amplitude of 0·1 mm.

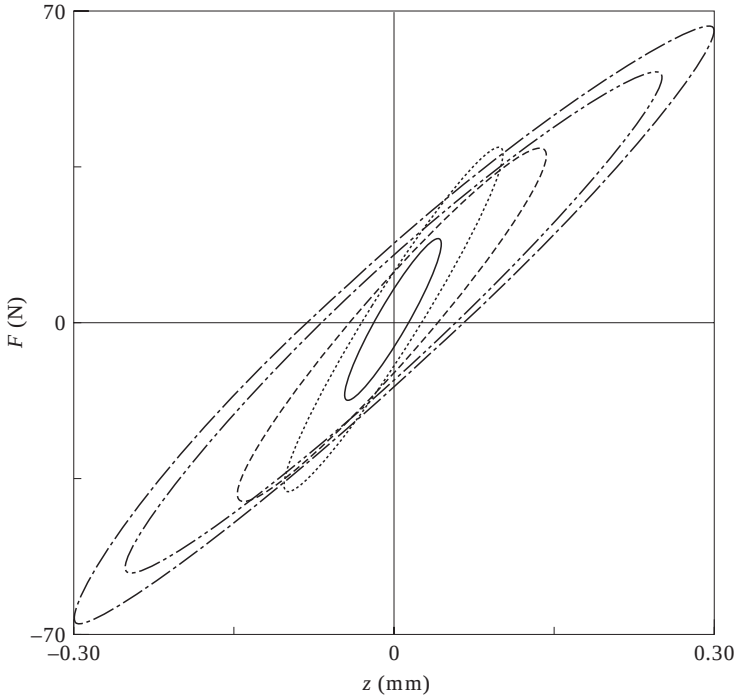

Figure 5. Mechanical hysteresis loops at 60 Hz with different amplitudes of deformation: ——, 0·05 mm; · · ·, 0·1 mm; ----, 0·15 mm; – · · –, 0·25 mm; – · –, 0·30 mm.

To study the dependence of the dynamics characteristics on the deformation amplitude, tests were conducted at a particular frequency with varying amplitudes. Figure 5 shows the hysteresis loops for various deformation amplitudes at a particular excitation frequency. It is clear from Figure 5 that, the dynamics stiffness of the specimen is amplitude-dependent and has a softening type characteristic. Therefore, it is proposed to model the restoring force (F_s) of the specimen as

$$F_s(z) = k_{dyn}z = [a - bZ^q]z; \tag{1}$$

where k_{dyn} is the dynamic stiffness and Z is the amplitude of deformation (z) with a, b and q as constants. These constants are determined by using the method of least squares to fit the experimental data on k_{dyn} obtained from the backbone curves of the hysteresis loops shown in Figure 5. The numerical values of these constants are obtained as follows: $a = 1476917{\cdot}4$ N/m, $b = 2839317{\cdot}7$ N/m$^{1{\cdot}1}$ and $q = 0{\cdot}1$. The values of k_{dyn} are seen to be greater than the static stiffness.

Figure 6 shows the variation of the specific damping energy (D_s = area of the loops shown in Figure 5) with the deformation amplitude (Z) at a particular frequency. This figure suggests that D_s is approximately proportional to $Z^{1{\cdot}5}$. Thus the entire rate-dependent damping force cannot be the linear hysteretic type for which D_s is proportional to Z^2. It is known that for Coulomb damping, D_s varies linearly with Z. Therefore, first it is proposed to model the

damping force (F_d) of the specimen, by a combination of hysteretic and Coulomb damping, as

$$F_d(\dot{z}) = f_c \operatorname{sgn}(\dot{z}) + (h/\omega)\dot{z}; \tag{2}$$

where h is the linear hysteretic damping coefficient, f_c is the limiting value of the Coulomb damping force, the dot at the top denotes the time-derivative and

$$\operatorname{sgn}(\dot{z}) = \begin{Bmatrix} +1 & \text{if} & \dot{z} > 0 \\ -1 & \text{if} & \dot{z} < 0 \\ 0 & \text{if} & \dot{z} = 0 \end{Bmatrix}.$$

With the damping force F_d given by equation (2), the specific damping energy D_s comes out as

$$D_s = \pi h Z^2 + 4 f_c Z. \tag{3}$$

The numerical values of h and f_c are obtained so as to fit equation (3) to the data points of Figure 6 in the sense of least square error. The numerical values so obtained are $h = 2{\cdot}11 \times 10^{-3}$ kg/s^2 and $f_c = 1{\cdot}5$ N.

It should be noted here that the idealized (constant) Coulomb damping, modelled by sgn ($\dot{z}$), results in sharp corners in the hysteresis loop due to a sudden (discontinuous) change in the value of the damping force at the limits of deformation during a cycle. Such sharp corners are, however, not discernible in Figure 5. This is not surprising. Due to various contributions of the molecular friction and effects of the fillers in the elastomer, the friction force does vary with both frequency and amplitude. The behaviour, in fact, is distinctly different from that seen in structural materials [14].

Following the dry friction characteristics of polymeric seals reported in reference [15], it is now proposed to modify equation (2) as follows:

$$F_d(\dot{z}) = F_c(\dot{z}) + F_h(\dot{z}) = [f_c + C_1 \mathrm{e}^{-C_2|\dot{z}| - C_3|} - (f_c + C_1 \mathrm{e}^{-C_2 C_3}) \mathrm{e}^{-C_4|\dot{z}|}]$$

$$\times \operatorname{sgn}(\dot{z}) + (h/\omega)\dot{z}, \tag{4}$$

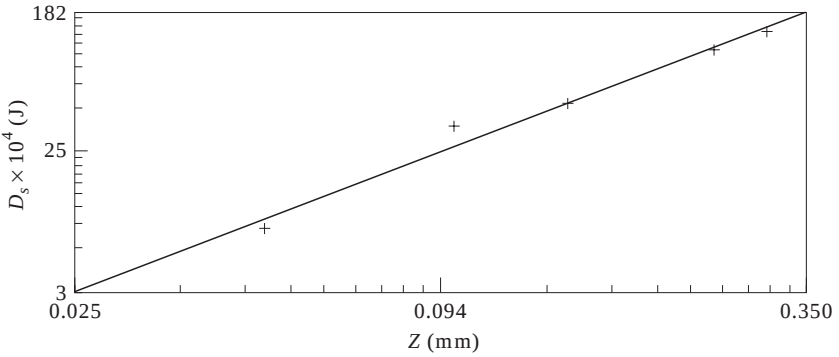

Figure 6. Variation of the specific damping energy with the deformation–amplitude at 60 Hz.

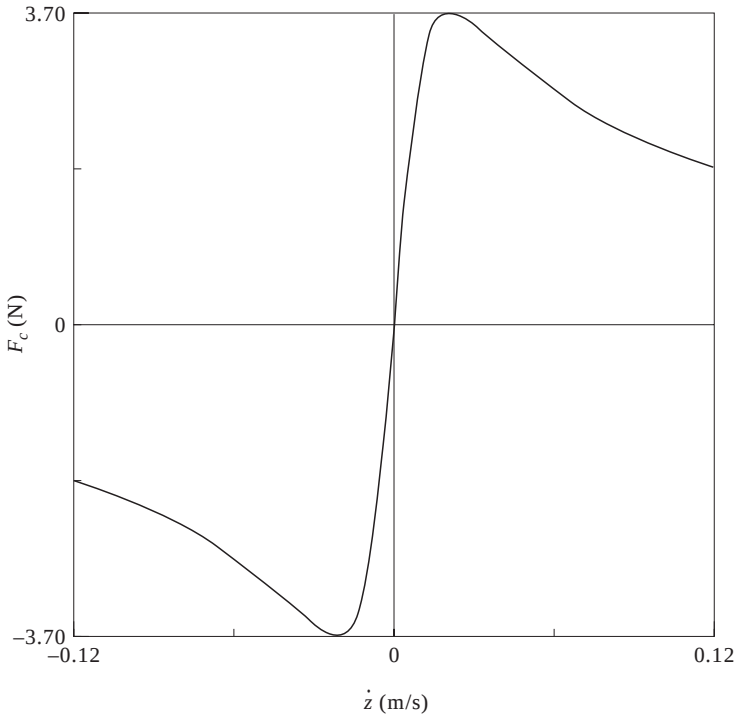

Figure 7. Variation of the Coulomb friction force with the rate of deformation.

where F_c represents the Coulomb damping force and F_h is the hysteretic damping force with C_1, C_2, C_3 and C_4 as constants. After a few trials, the following numerical values for these constants (for the specimen under experimentation) were obtained: $C_1 = 3{\cdot}5$ N, $C_2 = 20$ s/m, $C_3 = 0{\cdot}01$ m/s and $C_4 = 90$ s/m. With these values and $f_c = 1{\cdot}5$ N, the plot of F_c versus $\dot{z}$ is shown in Figure 7.

To check the validity of the proposed model (i.e., equations (1) and (4)), hysteresis loops are simulated by plotting $F(=F_d + F_s)$ versus z with $z = Z\cos(\omega t - \phi)$ at two different frequencies. The numerical values of various parameters like a, b, q, f_c, h, C_1 etc., have already been mentioned. Two such loops and the corresponding ones obtained experimentally are shown in Figures 8 and 9. Similar close agreements were observed for other frequencies and amplitudes of deformation [11]. The specific damping energy predicted by the mathematical model was seen to be proportional to $Z^{1{\cdot}48}$.

With the proposed mathematical model, the deformation of the specimen is governed by the following differential equation:

$$m\ddot{z} + F_s(z) + F_d(\dot{z}) = -m\ddot{y}, \tag{5}$$

where m is the isolated mass, $y = Y\cos\omega t$ is the base displacement and F_s and F_d are given by equations (1) and (4) respectively. The steady state harmonic transmissibility is given by $T = X/Y = [y + z]_{max}/Y$. It should be noted that such a model is valid only for harmonic (displacement) transmissibility neglecting super- and sub-harmonics, i.e., with $z = Z\cos(\omega t - \phi)$.

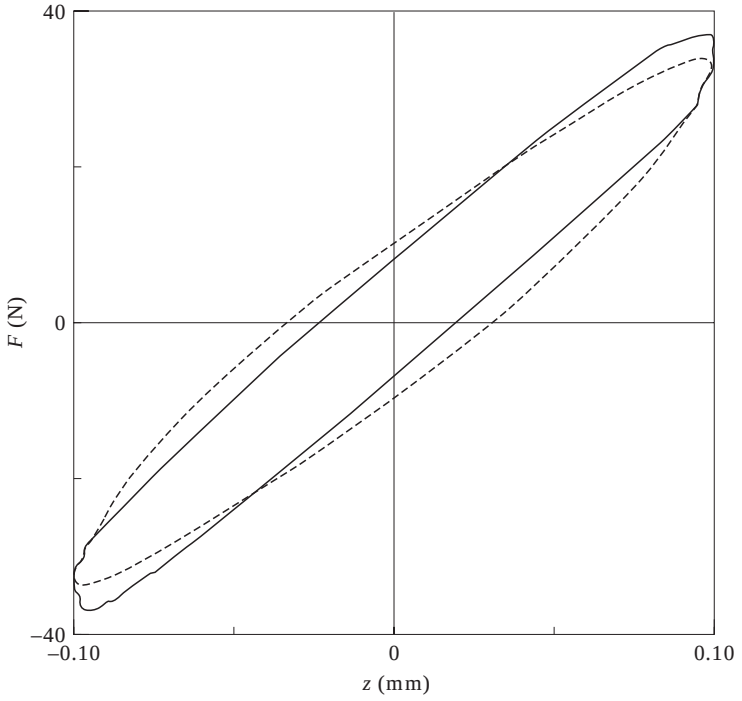

Figure 8. Comparison of mechanical hysteresis loops with 0·1 mm deformation amplitude at 50 Hz: ——, simulated by equation (4); ----, experimentally obtained.

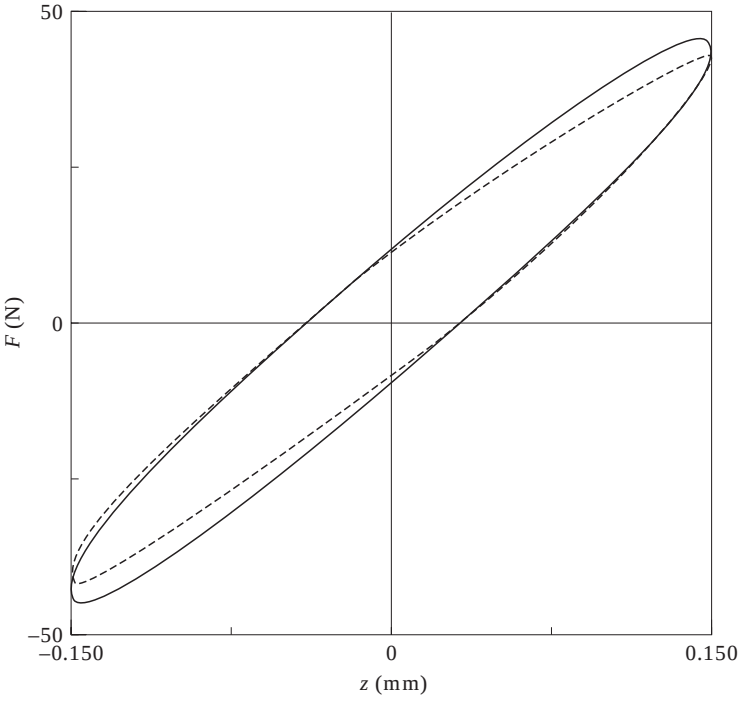

Figure 9. Comparison of mechanical hysteresis loops with 0·15 mm deformation amplitude at 120 Hz: ——, simulated by equations (1) and (4); ----, experimentally obtained.

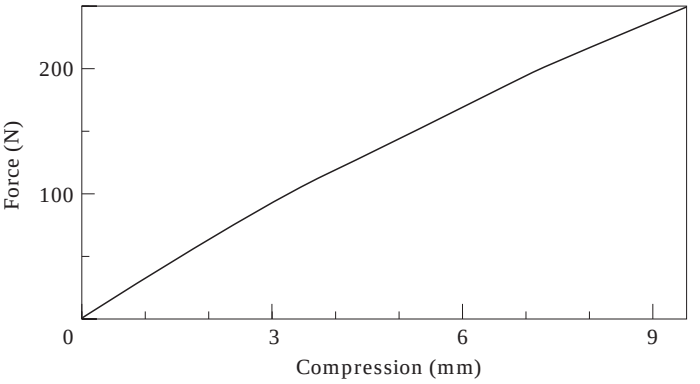

Figure 10. Static force–deformation characteristic during compression test of the bonded rubber spring specimen X20.

3.2. BONDED RUBBER SPRINGS

Figure 10 shows the force–deformation curve as obtained from the static test. Again a slight softening type characteristic is exhibited. The static stiffness starts with a value 33·3 kN/m and falls to 26·4 kN/m at the higher range of deformation. The harmonic displacement transmissibility (T) versus the frequency ratio Ω ($=\omega/\omega_n$ with ω_n as the linear natural frequency) plots with various base amplitudes are shown in Figure 11. The mass being isolated $m = 2{\cdot}1$ kg.

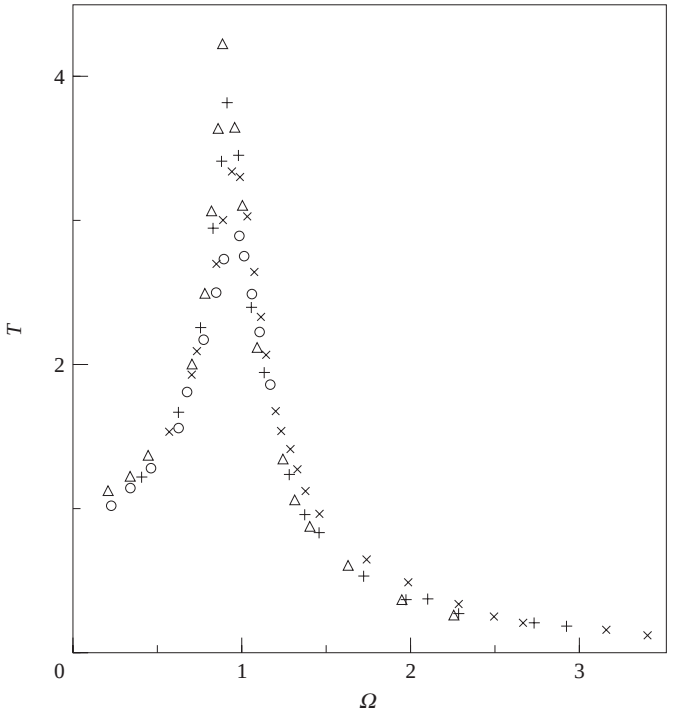

Figure 11. Variation of the harmonic displacement transmissibility with the frequency ratio at different base amplitudes (mm): ○, (0·2); ×, (1); +, (2); △, (3 and 3·5).

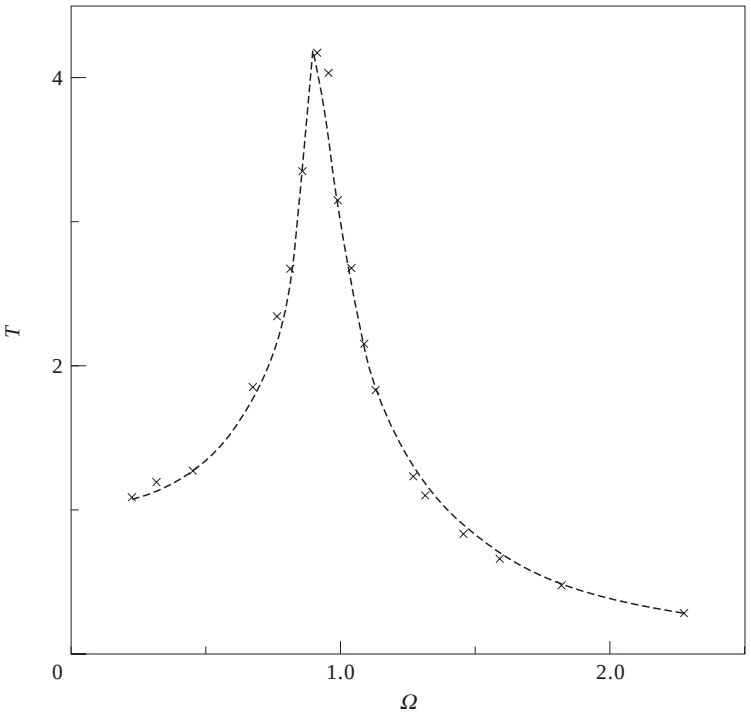

Figure 12. Comparison of transmissibility plots with 3·0 mm base amplitude: ×, experimentally obtained; ----, simulated by equations (6) and (7).

In the first step, the transmissibility curve with the minimum base amplitude (i.e., 0·2 mm in Figure 11) is considered and the non-linear effects neglected. The peak frequency (where the transmissibility is maximum) was found to be 22 Hz. One assumes this as the linear natural frequency of the system. This assumption is not very erroneous for the small amount of damping revealed by the narrow band width of the transmissibility plot. With $\omega_n = 2\pi \times 22$ rad/s and $m = 2{\cdot}1$ kg, the dynamic stiffness k_{dyn} is obtained as $k_{dyn} = 40{\cdot}125$ kN/m which, as expected, is more than the static stiffness. The viscous (linear) damping factor (ζ) is then obtained from the value of the resonance transmissibility (T_r), i.e., the transmissibility at $\Omega = 1$, using the standard result [1] is $\zeta = 1/2\sqrt{T_r^2 - 1}$ which comes out as 0·1768. Thus, the viscous damping coefficient $c = 2\zeta(k_{dyn}m)^{1/2} = 102{\cdot}6$ Ns/m.

To characterize the non-linear effects, one first observes from Figure 11 that with increasing base-amplitude, the peak transmissibility increases considerably with a slight change in the peak frequency. The changes in both these quantities saturate beyond a base-amplitude of 3 mm. The change in the peak frequency is mainly governed by the non-linearity in stiffness while that in the peak transmissibility is affected predominantly by the non-linearity in damping. The decrease in the peak ($\approx$natural) frequency with increasing deformation amplitude suggests a weak, softening type non-linearity in the stiffness. Similarly, the increase

in the peak transmissibility with increasing deformation amplitude can be modelled by providing a non-linear damping force with a negative coefficient.

Assuming symmetric behaviour in tension and compression, as a first trial cubic non-linear terms are used and the equatioin of motion for m is written as

$$m\ddot{z} + k_{dyn}z + \alpha z^3 + c\dot{z} + \beta\dot{z}^3 = -m\ddot{y}, \tag{6}$$

where $\ddot{y} = -\omega^2 Y \cos \omega t$ is the acceleration of the base. The linear parameters k_{dyn} and c have already been determined. The non-linear coefficients α and β are suitably adjusted so that the displacement transmissibility $T = [y + z]_{max}/Y$ matches the experimentally obtained values for $Y = 3$ mm. Equation (6) can be either numerically integrated (with trial values of α and β) using Runge–Kutta method or solved by the harmonic balance method [9]. The best values for α and β turn out to be $\alpha = -0{\cdot}0892$ N/mm^3 and $\beta = -25{\cdot}82$ Ns^3/m^3. The theoretical and experimental transmissibility plots, shown in Figure 12, match quite well. However, with the same values of α and β, if the amplitude of base displacement Y is changed to 2 mm, then the theoretical and experimental transmissibility values (especially the peak values) differ considerably as shown in Figure 13.

By proposing to replace the cubic damping term by quadratic type non-linearity and modifying equation (6) as follows:

$$m\ddot{z} + k_{dyn}z + \alpha z^3 + c\dot{z} + \beta\dot{z}|\dot{z}| = -m\ddot{y}. \tag{7}$$

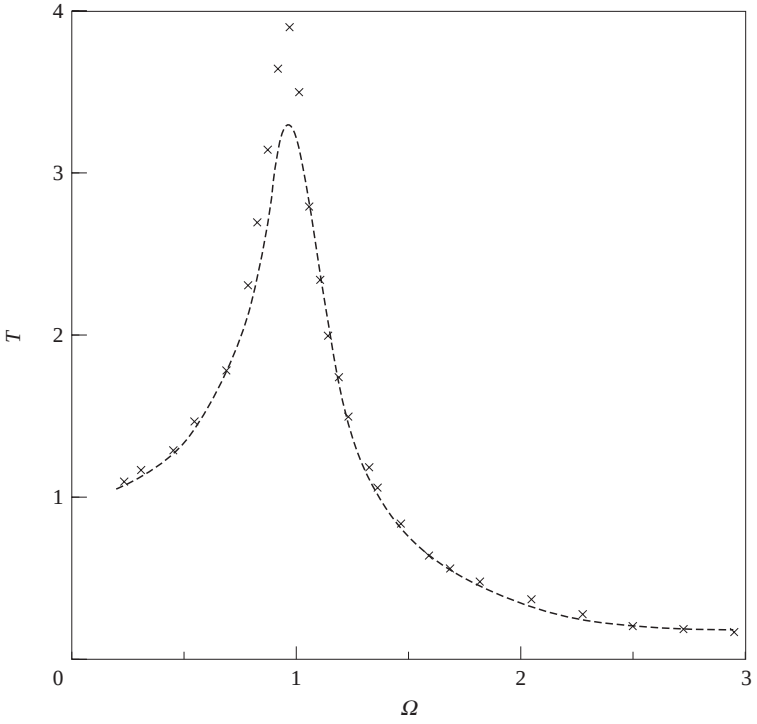

Figure 13. Comparison of transmissibility plots with 2·0 mm base amplitude: ×, experimentally obtained; ----, simulated by equation (6).

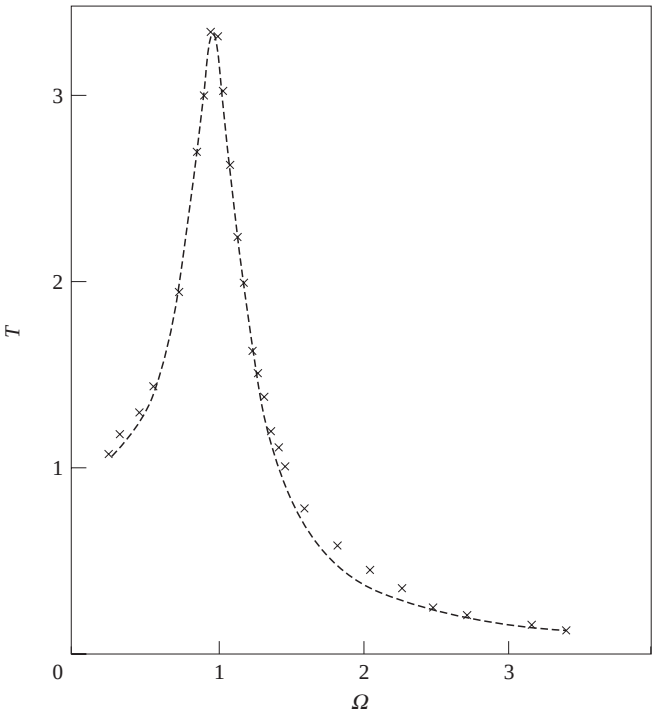

Figure 14. Comparison of transmissibility plots with 1·0 mm base amplitude: ×, experimentally obtained; ----, simulated by equation (7).

The transmissibility values obtained after numerical integration of equation (7) match closely the experimental values with $Y = 3$ mm for the following values: $\alpha = -0{\cdot}071$ N/mm^3 and $\beta = -0{\cdot}243$ Ns^2/m^2. With these values of α and β, the simulated (from equation (7)) and experimental transmissibility plots match very closely for all values of $Y \leqslant 3$ mm [12]. Figures 14 and 15 show two such plots for $Y = 1$ mm and 2 mm respectively.

Thus, the following constitutive equation

$$F(z, \dot{z}) = F_s(z) + F_d(\dot{z}) = k_{dyn}z + \alpha z^3 + c\dot{z} + \beta\dot{z}|\dot{z}|, \tag{8}$$

with $k_{dyn} = 40{\cdot}125$ N/mm, $\alpha = -0{\cdot}071$ N/mm^3, $c = 102{\cdot}6$ Ns/m and $\beta = -0{\cdot}243$ Ns^2/m^2 can be used to model the bonded rubber spring up to a fairly high level of deformation. It is known that the variation of the non-linear natural frequency (ω_{nl}) with the amplitude of motion for a linear plus a cubic restoring force is given by [16]

$$\omega_{nl}/\omega_n \approx 1 - \tfrac{3}{8}\frac{\alpha a^2}{k_{dyn}}, \tag{9}$$

where ω_n is the linear natural frequency and a is the amplitude of motion. It may be pointed out that the peak frequencies obtained from the experiment agree quite well with ω_{nl} obtained from equation (9) with $\alpha = -0{\cdot}071$ N/mm^3. The experimental results shown in Figure 10 demonstrated a saturation effect for

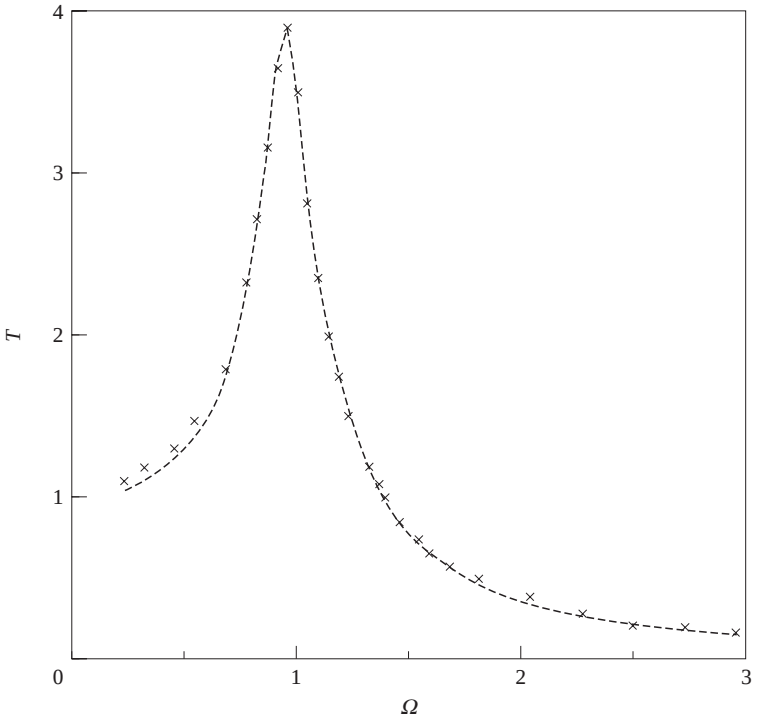

Figure 15. Comparison of transmissibility plots with 2·0 mm base amplitude: ×, experimentally obtained; ----, simulated by equation (7).

$Y > 3{\cdot}5$ mm. This behaviour can be modelled only after including higher order terms like γz^5 and $\delta \dot{z}^5$ with $\gamma > 0$, $\delta > 0$ in equation (8).

4. CONCLUSIONS

The non-linear dynamic constitutive equation of an elastomeric isolator can be modelled through two different approaches depending on the type of information needed. In order to simulate the experimentally obtained hysteresis loops, a combination of a linear hysteretic and a varying Coulomb damping is required. The dynamic stiffness, which is more than the static stiffness, can be modelled with a weak, softening characteristic. An assumed polynomial form of the constitutive equation can simulate the transmissibility characteristics. The accuracy and range of validity of the model depend on the chosen values of different exponents in the polynomial. The non-linearity is more predominant in the damping characteristic as compared to that in the stiffness characteristic.

REFERENCES

1. A. K. Mallik 1990 *Principles of Vibration Control*. New Delhi: Affiliated East–West Press (P) Ltd.
2. E. F. Göbel 1974 *Rubber Springs Design*. London: Newnes-Butterworth.

3. R. D. Corsaro and L. H. Sperling 1990 *Sound and Vibration Damping with Polymers*. Washington, D.C.: American Chemical Society.
4. J. Harris and A. Stevensen 1986 *Rubber Chemistry and Technology* **59**, 740–764. On the role of non-linearity in the dynamic behaviour of rubber components.
5. J. Harris 1987 *Rubber Chemistry and Technology* **60**, 870–887. Dynamic testing under non-sinusoidal conditions and the consequences of non-linearity on service performance.
6. M. L. Tinker and M. A. Cutchins 1992 *Journal of Sound and Vibration* **157**, 7–18. Damping phenomenon in a wire robe vibration isolation system.
7. N. Nakajima and E. A. Collins 1978 *Rubber Chemistry and Technology* **51**, 110–116. Viscoelastic properties of SBR containing particles of cross-linked polysterene.
8. A. J. Medalia 1987 *Rubber Chemistry and Technology* **60**, 437–523. Effect of carbon black on dynamic properties of rubber vulcanizates.
9. B. Ravindra and A. K. Millik 1994 *Journal of Sound and Vibration* **170**, 325–337. Performance of non-linear vibration isolators under harmonic excitation.
10. T. J. Royston and R. Singh 1996 *Journal of Sound and Vibration* **194**, 295–316. Optimization of passive and active non-linear vibration mounting systems based on vibratory power transmission.
11. V. Kher 1995 *M. Tech. Dissertation*, *IIT Kanpur*. Modelling of non-linear rubber isolators.
12. M. Puri 1996 *M. Tech. Dissertation*, *IIT Kampur*. Dynamic characterization of metal bonded rubber isolators.
13. J. E. Ruzicka and T. F. Derby 1971 *Influence of Damping in vibration isolation*, **SVM-7**. Washington, D.C.: The Shock and Vibration Information Center.
14. A. R. Payne 1964 *Rubber Journal* **146**, 36–49. The role of hysteresis in polymers.
15. B. S. Nau 1987 *Rubber Chemistry and Technology* **60**, 381–486. The state of the art rubber seal technology.
16. D. W. Jordan and P. Smith 1987 *Nonlinear Ordinary Differential Equations*. Oxford: Clarendon Press; second edition.